Nuclear Materials and Energy 34 (2023) 101386

Contents lists available at ScienceDirect

Nuclear Materials and Energy

journal homepage: www.elsevier.com/locate/nme

Analysis of edge transport in L-mode negative triangularity TCV discharges

P. Muscente [a,b], P. Innocente [b], J. Ball [c], S. Gorno [c], the TCV team[1], the EUROfusion MST1 team[2]

[a] Centro di Ateneo "Centro Ricerche Fusione" c/o Consorzio RFX, Padua University, Italy
[b] Consorzio RFX, Italy
[c] Ecole Polytechnique Fédérale de Lausanne (EPFL), Swiss Plasma Center (SPC), CH-1015 Lausanne, Switzerland

ARTICLE INFO

Keywords:
Negative triangularity
Power exhaust
Edge plasma transport
TCV
SOLEDGE2D-EIRENE

ABSTRACT

One of the major problems for future tokamak devices are ELMs (Edge Localized Modes) as they can lead to large, uncontrolled heat fluxes at the machine targets. For this reason, different techniques and alternative magnetic configurations are under study to mitigate or avoid these phenomena. One of the most promising among these studies is the Negative Triangularity (NT) configuration, which exhibits a global confinement comparable with H-Mode operation and, staying in L-mode, could enable an easier power exhaust dissipation due to a possible bigger heat flux decay length with respect to the conventional Positive triangularity (PT) H-mode. In this work, the fluid code SOLEDGE2D-EIRENE is used to study edge transport. Studies are made on discharges performed in the TCV device (Tokamak à configuration variable), which can create a variety of different plasma geometries thanks to 16 independently powered poloidal field coils and its open vacuum vessel. In order to understand if and how power and particle exhaust in NT differs with respect to those of the PT shape, four discharges in single null magnetic divertor configuration with fixed lower triangularity ($\delta_{bot} = +0.5$) but with different upper triangularity (from $\delta_{up} = -0.28$ to $\delta_{up} = +0.45$) have been modelled. All of them are ohmically heated, L-mode deuterium plasmas, and in the high recycling regime. Moreover, these discharges were previously used in [4] to measure the heat flux decay length by IRT (Infrared Thermography), allowing us to make comparisons with modelling results.

1. Introduction

Different techniques and alternative magnetic configurations are under study to mitigate or avoid the dangerous ELM instability. It has been demonstrated that techniques, such as RMP (Resonant Magnetic Perturbations) [14] and operating regimes with high ELMs frequency at reduced amplitude [15,16], are able to mitigate ELMs, avoid plasma facing components (PFC) melting and reduce erosion to an acceptable level, whilst remaining in a good H-mode performance range. Other studies are focused on developing different regimes or magnetic configurations that do not feature ELMs, such as EDA (Enhanced D-Alpha H-mode) [17], QCE (Quasi Continuous Exhaust) [18], QH-Mode (Quiescent H-Mode) [19] and Negative Triangularity (NT). In particular, NT is one of the most promising among the different regimes or magnetic configurations that do not feature ELMs [1,2]. This configuration, thanks to a low electron heat transport in the core, achieves the confinement necessary for a fusion reactor though it does not develop an edge transport barrier [13]. Additionally, thanks to the fact that this configuration does not need to reach the H-mode, the power crossing the last close flux surface (LCFS), P_{SOL}, does not need to be above the L-H power threshold, avoiding limits on the core radiation. Finally, we can suppose that NT could comply with the heat flux decay length (λ_q) trend found in studies presented in reference [3]. If so, Negative triangularity, staying in L-mode, could enable an easier power exhaust dissipation due to a possible bigger λ_q with respect to the conventional PT H-mode.

The aim of this work is to investigate the power exhaust and edge transport behaviors of the NT with respect to the PT in L-mode. An upper triangularity scan was performed in TCV in order to study the heat flux decay length inferred from IRT [4]. Here, we study the same experiments using data from Thomson Scattering (TS), Langmuir Probes (LP), bolometry and spectroscopy. Further, we use the transport edge code SOLEDGE2D-EIRENE [5,6] to understand how triangularity affects particle and heat perpendicular transport in the edge of the plasma. The code is suited to treat complex geometries and configurations due to the penalization technique implementation [7], which allows extending the simulation domain to the whole PFC.

E-mail address: paola.muscente@igi.cnr.it (P. Muscente).

[1] See the author list of H. Reimerdes et al 2022 Nucl. Fusion 62 042018.
[2] See author list of B. Labit et al 2019 Nucl. Fusion 59 086020.

https://doi.org/10.1016/j.nme.2023.101386
Received 30 June 2022; Received in revised form 10 January 2023; Accepted 7 February 2023
Available online 10 February 2023

In the following sections, we first describe the experimental data analysis and then the edge modelling setup and simulations results, comparing them also with the study by IRT in reference [4].

2. Experimental data set

The pulses under analysis are in single null magnetic divertor configuration with fixed lower triangularity, δ_{bot}=+0.5, and δ_{up}

from −0.28 to +0.45. These discharges were used in a previous study about the heat flux decay length [4] allowing us to have a results comparison. In Fig. 1, equilibria given by the magnetic equilibrium reconstruction LIUQE code [8] are shown. All discharges are ohmically heated and in L-mode deuterium plasmas in the high recycling regime, i.e. the electron temperature at the targets is between 10 eV and 20 eV. The global plasma parameters, shown in Table 1, are the same for all pulses. Other parameters, such as the mean electron density (n_e), the elongation (κ), the grazing angle and P_{SOL}, are fairly constant, allowing us to compare all cases independently of these parameters, see Table 2. For more details about the pulses please refer to reference [4].

3. Data analysis

Experimental data can give qualitative information on how triangularity affects transport at the edge of the plasma. Fig. 1 shows the diagnostics used for the following analysis.

The H-α emission, which is normally localized mostly in the divertor region, shows that the deuterium influx changes with δ_{up}. Fig. 2 shows the emission collected by the photodiode (PD), which intersects the outer leg of the LCFS in the same position for all pulses under analysis (see Fig. 1), giving information about the region around the outer strike point. We see that at the time instant studied, the emission decreases going from PT to NT configuration, suggesting a lower particle transport with the decrease of the upper triangularity. The comparison between cases can be done since the average density is mainly the same for all the four cases. This is confirmed also by the decrease of the ion saturation current with the decrease of δ_{up}. $J_{sat,i}$ is collected by Langmuir probes [9] at the targets. To see clearly this behavior, we decide to take into account the $J_{sat,i}$ dependency on electron density with the help of the 2-point model [10]. We know that $J_{sat,i} \propto n_t\sqrt{T_t}$ and in the high recycling regime $n_t \propto n_u^3$ and $T_t \propto 1/n_u^2$, and so it follows that $J_{sat,i} \propto n_u^2$, where u indicates upstream quantities (which is conventionally identify with the separatrix position at the outer mid-plane) and t indicates quantities at the target. Because we do not have a reference data for the upstream electron density, we use the average values of Thomson Scattering data [11] near the separatrix (around ρ = 0.98), which could be considered reliable in estimating the upstream density. In Fig. 3, the integral of the saturation current on targets, divided by n_u^2 and normalized with respect to the maximum, is plotted against the upper triangularities. On both targets, it increases with the δ_{up} confirming our suspicions from the H-α emission: NT decreases the particle transport.

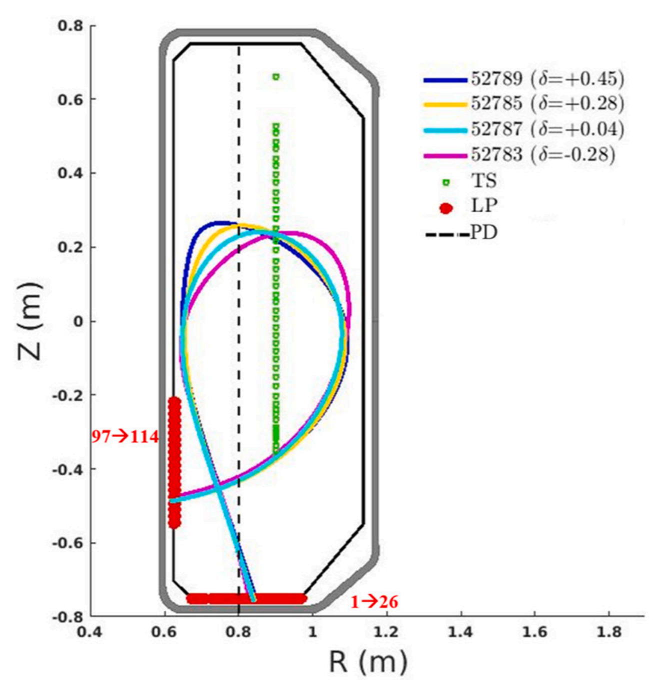

Fig. 1. Poloidal cross section of magnetic equilibrium reconstruction for the four pulses with different upper triangularity. In figure, the locations of the diagnostics used are also shown: Thomson scattering (TS) in green, Langmuir probes (LP) in the divertor region in red and photodiode vertical central line of sight (PD) in dashed black line. (For interpretation of the references to colour in this figure legend, the reader is referred to the web version of this article.)

Table 1
Parameters common to all pulses in the time interval of interest.

I_p (kA)	B_T (T)	Te (keV)	Ohmic power (kW)	Area (m^2)	Volume (m^3)	q95	q0
−240	−1.43	0.8	300	0.22	1.2	3–3.2	0.7–1

Table 2
The average electron density, n_e, the elongation, κ, the grazing angle and P_{SOL} are kept fairly constant between discharges with different upper triangularity.

Pulse #	δ_{up}	$n_{e,avg}$ (x10^{19} m^{-3})	κ	Grazing angle	P_{SOL} (kW)
52,789	+0.45	6.5	1.59	4.18	268
52,785	+0.28	7.2	1.64	3.85	263
52,787	+0.04	8.0	1.59	3.85	261
52,783	− 0.28	9.4	1.5	4.33	+0.45254

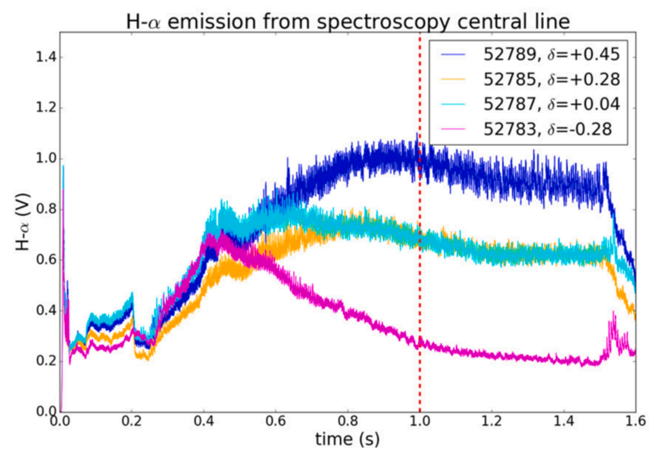

Fig. 2. H-α emission collected by the photodiode in a central vertical position for the four pulses. The red dashed line indicates the time instant around which the analysis is made. (For interpretation of the references to colour in this figure legend, the reader is referred to the web version of this article.)

Langmuir probe measurements are also analysed to explore the dependency of heat flux decay length, λ_q, on triangularity. Previous studies made with IRT found an increase of λ_q with the δ_{up} at the outer divertor target, while non-monotonic behaviour at the inner target was seen [4]. Fig. 4 shows the heat flux measurements collected at targets by LP fitted with a composition between one Gaussian distribution and two exponential functions, Fig. 4a and 4b. Data, normalised and centered with respect to the maximum value of the heat flux (Fig. 4c and 4d) show a non-monotonic trend on both targets. From this first analysis, it would

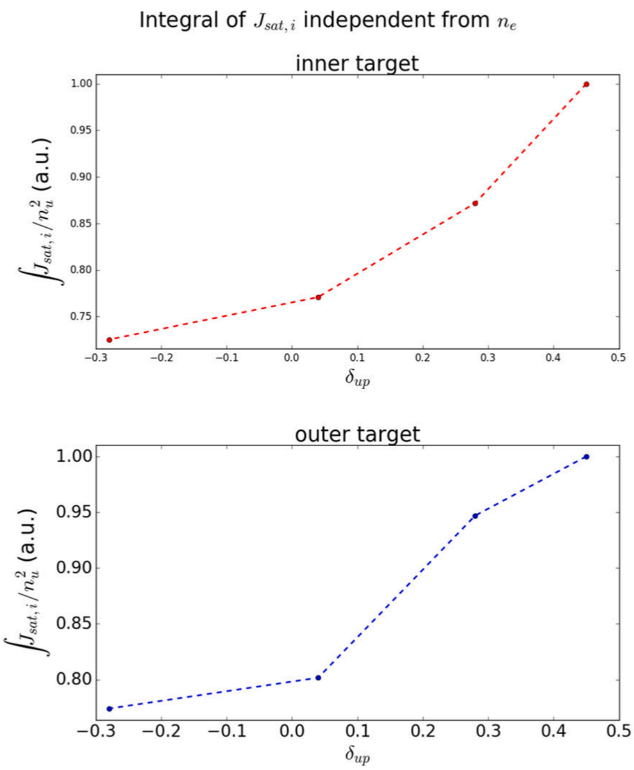

Fig. 3. Integral of the saturation current on targets from LP, divided by n_u^2 and normalized with respect to the maximum, plotted against the upper triangularity, for the inner and the outer target.

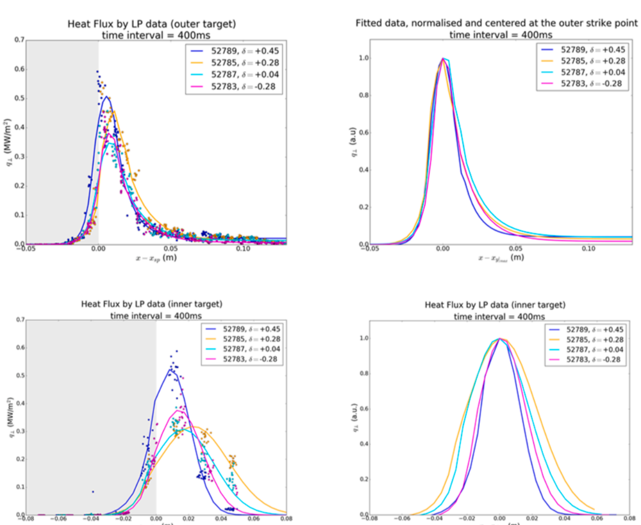

Fig. 4. Heat flux data by LP with fits on 400 ms time interval: a) on the outer target; b) on the inner one. The private region is colored in grey. Fitted data normalised and centered with respect to the maximum value of the heat flux: c) outer target; d) inner target.

seem that LP are not in agreement with IRT analysis [4] but we have to consider that the heat flux calculated from Langmuir probes measurements might be not accurate enough to see λ_q differences between pulses. On the contrary, in the following section, we will see that the edge modelling, constraint on the more reliable $J_{sat,i}$ measurements by LP, provides some indication about λ_q differences between pulses.

Experimental data analysis brings us to the conclusion that going toward the negative triangularity, there is a monotonic decrease in particle transport.

In the following sections, modelling studies and results are explained.

4. Modelling setup and results

In order to understand edge transport behaviors depending on the triangularity, we use the 2D fluid code SOLEDGE coupled with the EIRENE Monte-Carlo kinetic code for neutrals. Wall and divertor geometry are the same for all the four cases. Fig. 5 shows an example, for the negative δ_{up} case, of the meshgrid for SOLEDGE plasma fluid solver (Fig. 5a), which covers all the edge plasma volume extending outside the wall to provide the boundary constraint for the penalization method. In Fig. 5b is shown the EIRENE meshgrid, which overlays the SOLEDGE one in the plasma domain, while Fig. 5c shows the locations of the D_2 puffing valve and of the pump, which does not have a significant role in the particle balance because the TCV carbon wall itself plays the major role [21]. No drifts nor spatial magnetic field dependences are included in transport values. We investigated if the spatial inhomogeneity of the toroidal magnetic field module could have some influences on simulation results including the normalised $1/B_{toroidal}$ dependency: no effects at all were found and for this reason the simulations were done without any dependencies.

Since the modelling domain includes only a negligible portion of the plasma core, P_{SOL} is computed by subtracting from the ohmic heating the radiated power in the core in addition to that due to impurity, since simulations are performed in pure Deuterium. Impurity radiation is mostly localised out of the LCFS and we know to be mostly due to Carbon because of the carbon-wall of the device. All radiation power estimations are based on bolometry measurements [12]. The P_{SOL} values used, shown in Table 2, are split equally between electrons and ions. Thomson scattering data are used to tune transport profiles. In Fig. 6 an example of the matching between experimental data, which cover only the region inside the separatrix, and modelled profiles are shown for the cases with $\delta_{up}=\pm0.28$. Transport parameters have been kept radially non-uniform specifically in order to reproduce LP profiles on the outer target, in particular $J_{sat,i}$, the electron density and the electron temperature. In Fig. 7, profiles on the outer target for the negative δ case are shown.

The transport profiles, which allow to have a good match in shape and values of experimental data, are shown in Fig. 8. Focusing inside and at the separatrix, we see that particle diffusion decreases monotonically with δ_{up} from PT towards NT, while the heat diffusion does not show any particular trend. In particular, the negative δ case has exactly the same value $\chi_{i,e} = 1.0\ m^2/s$ as two of the positive cases. To investigate if triangularity affects more the particles or the heat diffusion not only at the separatrix but also in the whole near-SOL, we fixed before $\chi_{i,e}$ profile and then D profile in all cases. In χ-fixed cases, the $\chi_{i,e}$ profile chosen was the one which change out of the separatrix after $\sim \lambda_T$ for all the cases, which correspond to the cyan profile in Fig. 8, while the D profiles were

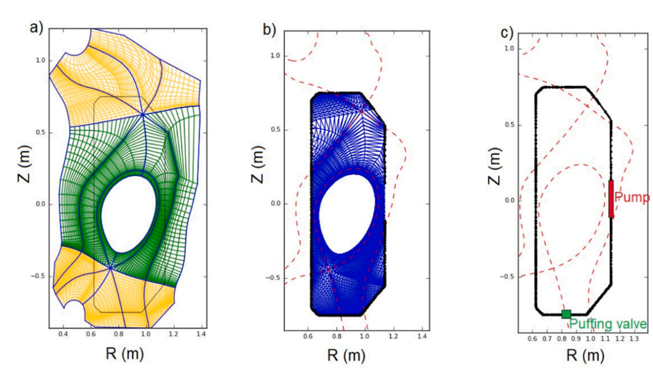

Fig. 5. Modelling meshes and wall: a) SOLEDGE2D quadrangles fluid mesh; b) EIRENE triangles mesh; c) gas-puffing and pump locations.

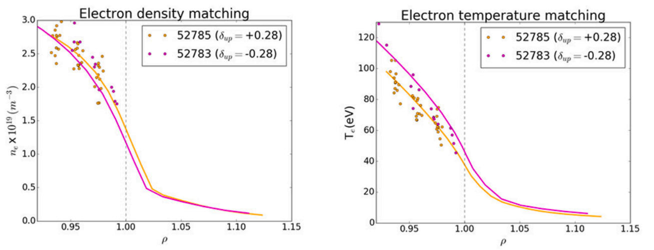

Fig. 6. Matching between TS data (dots) and modelled profiles (solid line) on the outer mid-plane for cases with $\delta_{up}=\pm0.28$.

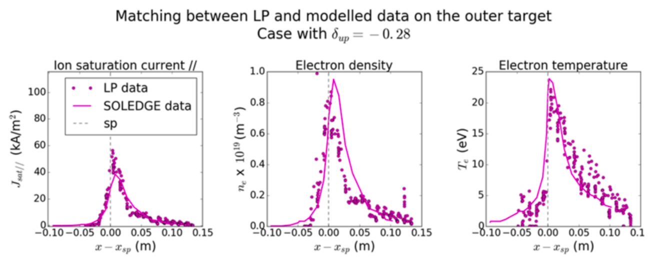

Fig. 7. Matching between LP profiles (dots) on the outer target and modelled profiles (solid line) for the negative triangularity case. The dashed line in grey indicates the strike point reference.

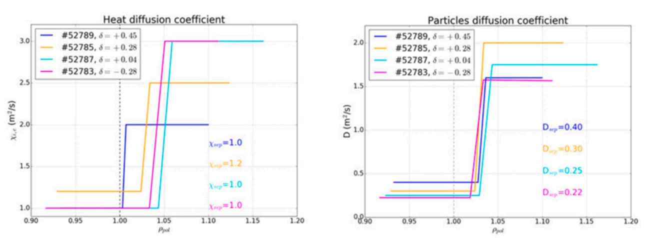

Fig. 8. Particles and heat transport profiles for the four cases under analysis.

left in ad hoc shapes. The D-fixed cases follows the same logic but with respect to λ_n, D profile chosen was the one in blue in Fig. 8, and ad hoc $\chi_{i,e}$ were used. Fixing $\chi_{i,e}$, the match between data and simulated profiles is good as before, see Fig. 9, only little change in shape is visible but its investigation is out of our purposes. On the contrary, fixing D simulated profiles do not match data as good as before. In particular, density profile at the outer mid-plane is overestimated, density and temperature at the outer target are overestimated and underestimated respectively, see Fig. 10.

We can conclude that triangularity affect more the particle transport than the energy transport in the near-SOL.

In the far-SOL no particular trend is found, both in particles and heat transport, but it has to be notice that experimental data available allow us to focus only on the near SOL. The coefficient values fixed in the far SOL were chosen to increase the diffusion in order to help the match of LP data on the targets but real values could be different.

The good match between profiles on the targets allows a reliable estimation of the heat flux decay length by SOLEDGE2D-EIRENE. Fig. 11 shows λ_q calculated by fitting the outer mid-plane $nT^{3/2}$ profile that, as for the λ_q obtained by using IRT [4], shows a monotonically increasing trend with δ_{up}.

5. Conclusions

In this work, in order to understand the power exhaust in Negative Triangularity with respect to the conventional Positive Triangularity shape in L-mode, an upper triangularity scan performed in TCV was

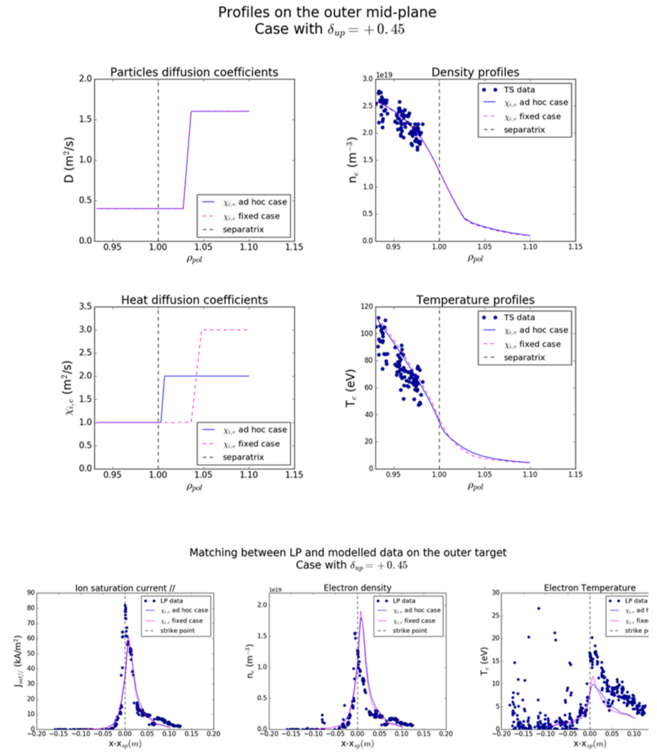

Fig. 9. On the top are shown outer mid-plane profiles, on the bottom targets profiles. We can see that the match between data and simulated profiles is good as before.

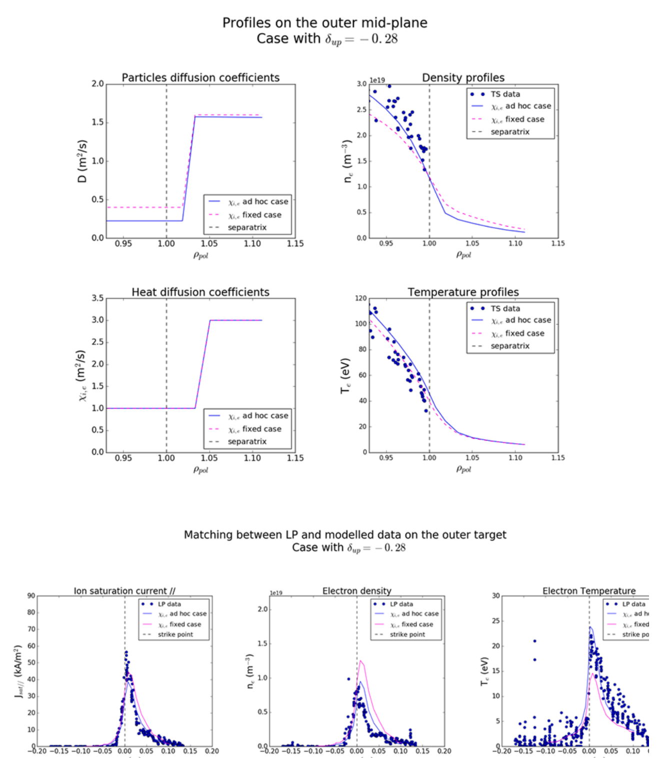

Fig. 10. On the top are shown outer mid-plane profiles, on the bottom targets profiles. We can see that the match between data and simulated profiles is good as before.

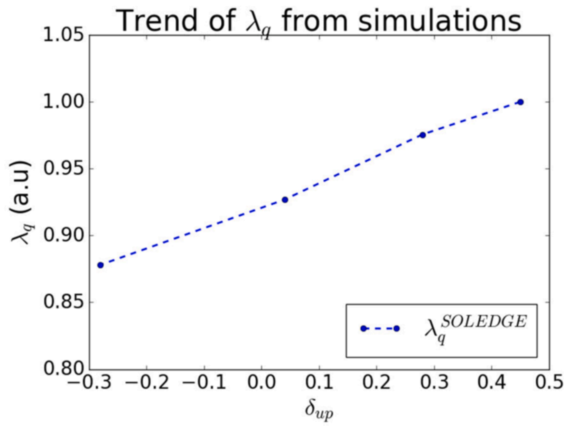

Fig. 11. λ_q on the outer mid-plane obtained by modeling fitting the $nT^{3/2}$ profile.

studied [4]. The pulses were in standard single null magnetic divertor configuration with fixed lower and variable upper triangularity. All of them were ohmically heated, L-mode deuterium plasmas and in the high recycling regime.

We analysed directly the experimental data and used the edge transport code SOLEDGE2D-EIRENE to investigate particle and heat diffusion and heat flux decay length behaviour.

Modelling results provide an explanation of the initial data analysis, showing that particle transport has a monotonic behaviour, decreasing towards NT, while the heat transport does not seem to depend on the triangularity. Moreover, the transport code highlights that λ_q on the outer mid plane increases monotonically with δ_{up}, which is consistent with the IRT analysis [4].

It is to notice that our analysis does not allow to have precise information about transport coefficient values in the far-SOL. In order to improve our studies, future works will be done on experiments with a more extensive diagnostics coverage [20].

The work presented here allowed us to characterise the edge transport in upper Negative Triangularity discharge, confirming that the NT affects not only the core transport but also edge transport. Future works will be dedicated to the comparison between PT H-mode and NT plasmas in order to compare relevant reactor conditions and understand if and how Negative Triangularity could provide improvements from the power exhaust point of view.

CRediT authorship contribution statement

P. Muscente: Conceptualization, Methodology, Software, Validation, Formal analysis, Investigation, Writing – original draft, Writing – review & editing, Visualization. **P. Innocente:** Conceptualization, Methodology, Writing – review & editing. **J. Ball:** Writing – review & editing, Supervision, Project administration. **S. Gorno:** Investigation, Data curation, Writing – review & editing.

Declaration of Competing Interest

The authors declare that they have no known competing financial interests or personal relationships that could have appeared to influence the work reported in this paper.

Data availability

Data will be made available on request.

Acknowledgments

This work has been carried out within the framework of the EUROfusion Consortium, funded by the European Union via the Euratom Research and Training Programme (Grant Agreement No 101052200 – EUROfusion). Views and opinions expressed are however those of the author(s) only and do not necessarily reflect those of the European Union or the European Commission. Neither the European Union nor the European Commission can be held responsible for them. This work was supported in part by the Swiss National Science Foundation. This work was performed with MARCONI-FUSION HPC. The required computational resources were allocated under the project EMCAD and TSVV2.

References

[1] A. Marinoni et al., 2021, Reviews of Modern Plasma Physics 5.1: 1-44.
[2] M. Kikuchi, et al., Nucl. Fusion 59 (2019), 056017.
[3] R. Maurizio, et al., Nuclear Fusion 61 (2) (2021), 024003.
[4] M. Faitsch, et al., Plasma Phys. Control. Fusion 60 (2018), 045010.
[5] H. Bufferand, et al., J. Nucl. Mater. 438 (2013) S445–S448.
[6] H. Bufferand, et al., Nucl. Fusion 55 (2015), 053025.
[7] A. Paredes, et al., J. Nucl. Mater. 438 (2013) S625.
[8] F. Hofmann, G. Tonetti, Nucl. Fusion 28 (1988) 1871.
[9] H. De Oliveira, Rev. Sci. Instrum. 90 (2019), 083502.
[10] C.S. Pitcher, P.C. Stangeby, Plasma Phys. Control. Fusion 39 (1997) 779.
[11] P. Blanchard, et al., JINST 14 (2019) C10038.
[12] J. Mlynar et al., 1999, Bolometry on the TCV Tokamak. No. REP_WORK. 1999.
[13] M.E. Austin et al., 2017, 59th APS-DPP Bulletin Bo4 2.
[14] T.E. Evans, et al., Phys. Rev. Lett. 92 (2004), 235003.
[15] Y. Kamada, et al., Plasma Phys. Control. Fusion 42 (2000) A247.
[16] J. Stober, et al., Nucl, Fusion 41 (2001) 1123.
[17] Greenwald, et al., Physics of Plasmas 6 (1999) 1943.
[18] M. Faitsch, et al., Nucl. Mater. Energy 26 (2021), 100890.
[19] K. Burrell, et al., Bull. Am. Phys. Soc. 44 (1999) 127.
[20] W. Han, et al., Nucl. Fusion 61 (2021), 034003.
[21] J. Wesson et al., 2011, Tokamaks, Vol. 149. Oxford university press, p.485-488.